



IMPACTS OF OCEAN-ATMOSPHERE INTERACTION PHENOMENA ON HYDROMETEOROLOGY OF THE GURUPI RIVER WATERSHED, EASTERN AMAZON

*Impactos de fenômenos da interação oceano-atmosfera na
hidrometeorologia da bacia hidrográfica do rio Gurupi,
Amazônia Oriental*

*Impactos de los fenómenos de interacción océano-atmosfera
en la hidrometeorología de la cuenca del río Gurupi,
Amazonía Oriental*

Dênis José Cardoso Gomes  

State University of Pará
deniss.feg@gmail.com

Norma Ely Santos Beltrão  

State University of Pará
normaely@uepa.br

Abstract: Extreme events impact in hydrometeorology of Amazonian watersheds. The objective of this research was to analyze the effects of climate extremes on rainfall and discharge variability in a watershed in Eastern Amazonia. Climatic indices, hydrometeorological and spatial data were acquired for the analysis of the watershed of the Gurupi river. Calculations of correlation, efficiency, detection of a difference in distribution, and trend of changes in hydroclimatic variability were applied, in addition to using the Rainfall Anomaly Index. There is a greater influence of the tropical Atlantic on precipitation, as well as precipitation on the Gurupi upper flow. Significant differences were detected in rainfall distribution, as well as increasing and decreasing trends. Regional climatology is marked by the highest (smaller) rainfall in the North (South), with extremes and anomalous years. The Gurupi basin is impacted by climate extremes. Evidence suggests vulnerability to the region's climate and the need for preventive measures.

Keywords: ENSO. Atlantic Dipole. Rainfall. Flow.

Resumo: Os eventos extremos impactam na hidrometeorologia de bacias hidrográficas amazônicas. O objetivo desta pesquisa foi analisar os efeitos de extremos climáticos da variabilidade da precipitação

e vazão em uma bacia hidrográfica na Amazônia Oriental. Os dados de índices climáticos, hidrometeorológicos e espacializados adquiriu-se para a análise da bacia hidrográfica do rio Gurupi. Aplicou-se cálculos de correlação, eficiência, detecção de diferença na distribuição, tendência de mudanças na variabilidade hidroclimática, além de utilizar o Índice de Anomalia de Chuva. Há maior influência do Atlântico tropical na precipitação, assim como a precipitação na vazão do Alto Gurupi. Foi detectada diferenças significativas na distribuição pluviométrica, assim como tendências de aumento e diminuição. A climatologia regional é marcada pelas maiores (menores) chuvas ao Norte (Sul), com extremos e anos anômalos. A bacia do Gurupi é impactada pelos extremos climáticos. Evidências sugerem a vulnerabilidade ao clima da região e necessitam de medidas para de prevenção.

Palavras-chave: ENOS. Dipolo Atlântico. Precipitação. Vazão.

Resumen: Eventos extremos impactan la hidrometeorología de las cuencas amazónicas. El objetivo de esta investigación fue analizar los efectos de los extremos climáticos sobre la variabilidad de la precipitación y el caudal en una cuenca de la Amazonía Oriental. Se adquirieron los datos de índices climáticos, hidrometeorológicos y espacializados para el análisis de la cuenca del río Gurupi. Se aplicaron cálculos de correlación, eficiencia, detección de diferencia en distribución, tendencia de cambios en la variabilidad hidroclimática, además de utilizar el Índice de Anomalia de Precipitación. Hay una mayor influencia del Atlántico tropical en la precipitación, así como la precipitación en el desagüe del Alto Gurupi. Se detectaron diferencias significativas en la distribución de las precipitaciones, así como tendencias de aumento y disminución. La climatología regional está marcada por las mayores (menores) precipitaciones del Norte (Sur), con extremos y años anómalos. La cuenca de Gurupi se ve afectada por los extremos climáticos. La evidencia sugiere vulnerabilidad al clima de la región y la necesidad de medidas preventivas.

Palabras clave: ENOS. Dipolo Atlántico. Precipitación. Tasa de flujo.

Submetido em: 18/03/2023

Aceito para publicação em: 10/07/2024

Publicado em: 14/07/2024



1. INTRODUCTION

Extreme events are generally the combination of the extreme occurrence of meteorological variables (rainfall, air temperature, and wind), hydrological (river level and flow), and oceanic (sea surface temperature). According to Ren et al. (2021), they are categorized into temperature extremes (heat waves and cold), hydroclimatic extremes (rainfall, floods, and droughts), and hurricanes, respectively. Olafsdottir et al. (2021) highlighted that climate change could increase extreme events, such as intense storms, becoming dangerous when they occur with greater frequency and intensity.

Several climatic mechanisms may be responsible for the intensification of these extreme events. One of the most studied and known in the world is the El Niño South Oscillation (ENSO), composed of the El Niño (EN) and La Niña (LN) phases formed in the Tropical Pacific Ocean (TP). The EN causes changes in the general circulation of the winds because, according to Hayashi et al. (2020), the de-intensification of the trade winds in the tropical region displaces smaller amounts of surface water from the TP, as well as decreases the upwelling of deep cold waters. Consequently, anomalous heating is indicated by the sea surface temperature (SST). This combination of ocean-atmosphere coupling factors alters the sea-level barometric field (TADESCHI et al., 2015), which modifies the Walker circulation patterns (YUN et al., 2021). As the Walker cell is the circulation of winds with ascending and descending branches along the tropical region (SIQUEIRA; MOLION, 2015), the EN generates some effects such as air subsidence movement over most of Northern Brazil and inhibition of uplift moisture to the atmosphere by air convection (NOBRE et al., 2019), delaying cloud formation and precipitation (BARICHIVICH et al., 2018). The LN has physical processes of formation and effects opposite to the EN, such as cooling of the oceanic waters of the TP, and upward movement of air in most of the Amazon and the Northern Northeast, among others (NOBRE et al., 2019).

According to Jahfer et al. (2017), climate variability in the Amazon is not only impacted by ENSO. The Atlantic Dipole is another climate modulator from the Tropical Atlantic (TA) that impacts the rainfall regime in the Northern region of Brazil (SOUZA et al., 2005; TOWNER et al., 2021), also consisting of positive phases (AD^+) and negative (AD^-). When the Tropical Northern Atlantic (TNA) and Tropical Southern Atlantic (TSA) climate indices reach abnormally warm and cold values, respectively, the large-scale system known as the Intertropical

Convergence Zone (ITCZ) moves meridionally to the Northern Hemisphere and causes strengthening in the convective activity of this region (TOWNER et al., 2020). Such atmospheric conditions are favorable to the emergence of AD⁺ due to its influence on the ITCZ, in which this phenomenon is eventually associated with cases of dry spells and droughts in some regions of the Amazon, such as the Eastern edge (transition zone between biomes). In the opposite scenario, i.e., AD⁻, anomalous warm TSA waters move the ITCZ to the Northern region of Brazil, contributing to greater air convection and consequently increasing rainfall (TOWNER et al., 2020).

The influence of these climatic phenomena on Amazonian rainfall (ARAÚJO et al., 2013) occurs through teleconnection (CAI et al., 2020). Climate teleconnection concerns the circulation of anomalous winds (ZHANG et al., 2022) associated with atmospheric pressure gradients that impact precipitation in remote areas (CAROLETTI et al., 2021) and can vary at different time scales (BAHAGA et al., 2019). However, the Eastern Amazon presents geoenvironmental aspects of transition zones, such as some areas under the influence of the sub-humid characteristics of the Cerrado biome (SALES; OLIVEIRA NETO, 2020). This makes monitoring of extreme droughts necessary (NIAZ et al., 2022) since humidity is reduced. Therefore, the spatialization of precipitation (COSTA et al., 2019) combined with the analysis of climatic mechanisms (SANTOS et al., 2019) contributes to identifying the surplus and absence of rain.

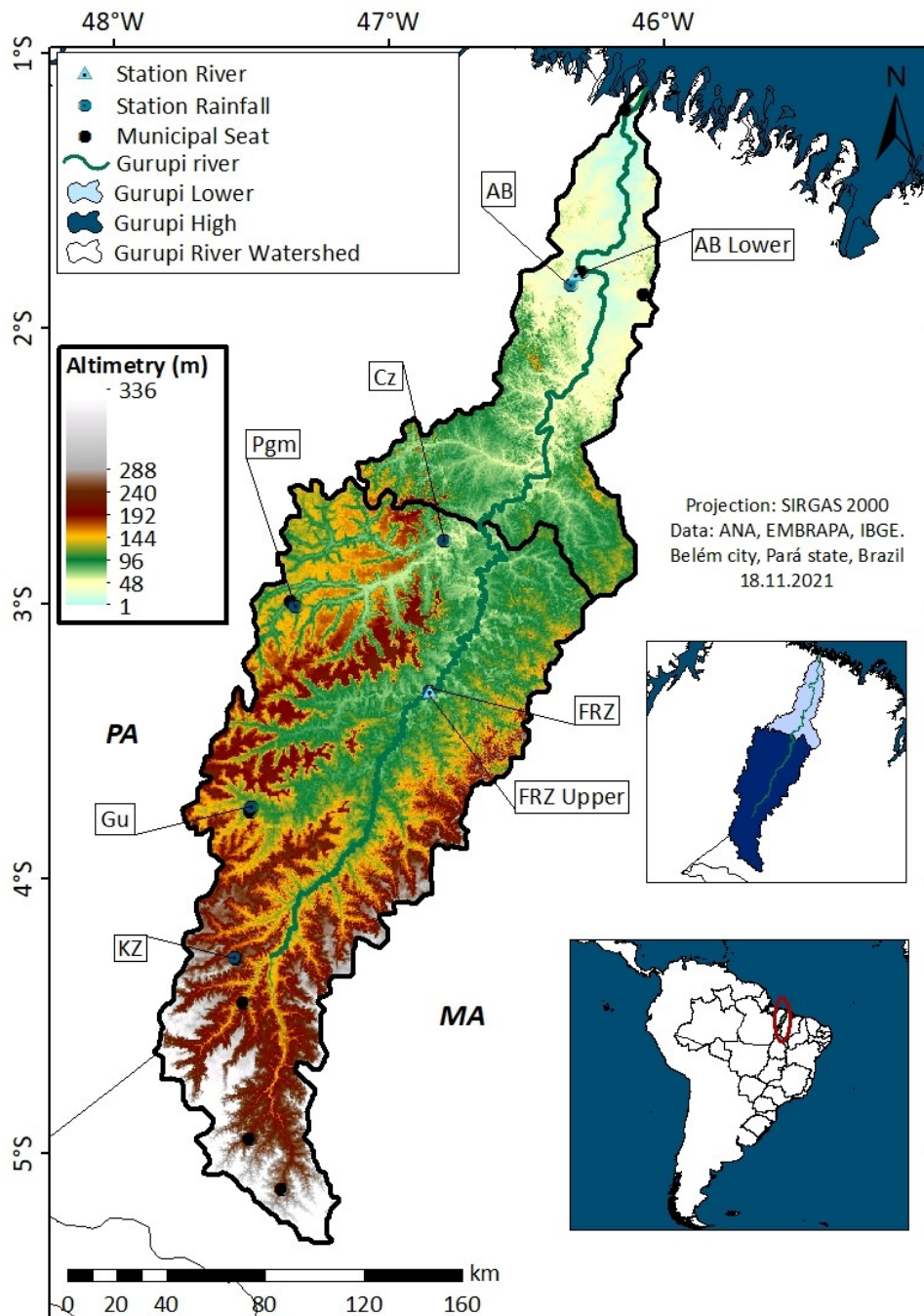
To verify the impacts of climatic anomalies of the TA and TP oceans on Amazon rainfall patterns, observing the temporal variability of fluviometric components at the level of watersheds becomes necessary (CAPOZZOLI et al., 2017) since many environmental disturbances are associated with rivers (TOWNER et al., 2020). Teleconnections with ENSO and Atlantic Dipole phenomena strongly affect the Eastern Amazon region (REBOITA; SANTOS, 2014). Although there are works that have addressed the influence of climatic phenomena on the hydrometeorological variability of the Amazon (PEDREIRA JUNIOR et al., 2020; BRITO et al., 2022) and Northeast Brazil (UVO et al., 1998; RODRIGUES et al., 2021), it is necessary to analyze how climatic mechanisms are influencing the hydrometeorological regime of a watershed in a biome transition zone. So, given the need to investigate these hydroclimatic interactions, this research aimed to analyze the effects of climatic mechanisms on the variability of precipitation and flow in a watershed in the Eastern Amazon.

2. METODOLOGY

2.1 – Study area

The Gurupi river watershed (GrW) is located (Fig. 1) in the Eastern Amazon, bordering the states of Pará (PA) and Maranhão (MA) with an area of approximately 35,875.0 km² where about 392,601 people live distributed over 11 municipal seats (ANA, 2015).

Figure 1 – Location of the study area: Gurupi River Watershed.



Source: Authors (2022). *MA-Maranhão State; PA-Pará State.

The regional ecosystem is characterized by a biome transition, where the forest cover is predominantly Amazon biome formed by ombrophilous forests, with some areas of continuous canopy savanna vegetation such as semideciduous seasonal forests that indicate the presence of cerrado (MMA, 2022). GrW's climate is marked by annual rainfall ranging from 1,450.0 mm – 2,650.0 mm, minimum and maximum air temperature of 24° and 33°C respectively, relative humidity of 85%, evapotranspiration of 1,400 mm, wind speed and direction of 2 m/s northeast (INMET, 2022). GrW has a well-defined relief with the largest highlands (192 m – 336 m) to the South and Southwest, a region marked by the Gurupi Upper (GU) where the headwaters (Gurupi Mountain Range) of the Gurupi River (700 km) are located to the Lower Gurupi (GL) characterized by the plains (1 m - 144 m) until it flows into the TA.

2.2 – Data acquisition

Climate indices (1980-2019) from SST anomalies were acquired from the National Oceanic and Atmospheric Administration (NOAA, 2021). The positive (EN) and negative (LN) phases of the ENSO phenomenon were done using the TP Oceanic Niño Index (ONI). Another climatic index used was the TNA and TSA SST to identify the Atlantic dipole phenomenon, in which they were classified based on NOAA data (2021) and the results of Jorge and Lucena (2018). ONI values are SST anomalies representing a continuous quarterly average (December, January, and February) that indicate the oscillations (heating/cooling) of a TP region (NOAA, 2022). EN (LN) events are defined when ONI values reach +0.5 °C (-0.5 °C), persisting for at least five months or longer (GONZALES; INGOL, 2021). In the TA, the development of the AD⁺ (AD⁻) phenomenon was defined when an SST gradient, i.e., anomalies between the TNA and TSA, reached values greater/equal to 0.2 °C (lower/equal to -0.2 °C) for at least four consecutive months (SOUZA et al., 2005). Precipitation data were obtained from the National Water Agency and Basic Sanitation rain gauges on the HidroWeb platform (ANA, 2021). Six (6) rainfall stations from the National Water Agency and Basic Sanitation (ANA) located along the GrW and two (2) rainfall stations in the Gurupi River were selected. However, due to the flaws in the observations (MELLO et al., 2017) and low spatial distribution density (RUEZZENE et al., 2021) of the hydrological stations, the criterion with a high percentage was taken into account (MENDES; ZUKOWSKI JUNIOR, 2019). The gap filling in the observations of the stations was



not performed due to the risk of compromising the data series, which can generate inconsistency and subjectivity in the analysis (NASCIMENTO et al., 2020). The precipitation distribution in GrW was based on the Climate Hazards Group InfraRed Precipitation with Stations (CHIRPS, 2021) dataset proposed by Funk et al. (2015), which has a spatial resolution of 0.05° (~ 5 km).

2.3 – Statistics and Data Processing

For the validation of the estimated data from the CHIRPS, the measured data from the rainfall stations were used (CAROLETTI et al., 2019) and the Pearson correlation (r). The application of Pearson correlation occurred in three moments. First, in the BioEstat 5.3 software (SANTOS et al., 2020), the normality test (Shapiro-Wilk) was performed for the hydroclimatic data (climate indices, precipitation, and flow). The data conform to a normal distribution ($p > 0.05$) for the TA climatic indices (TNA and TSA), as well as for four pluviometric stations: Alto Bonito (AB), Fazenda Rural Zebu (FRZ), Km-Zero (KZ), and Gurupizinho (Gu). However, the test revealed that the data for the climatic index TP (ONI) did not follow a normal distribution ($p < 0.05$). This was observed in two pluviometric stations, Paragominas (Pgm) and Cafezal (Cz), as well as in two fluvial stations, Alto Bonito (AB_{lower}) and Fazenda Rural Zebu (FRZ_{upper}), located in the GL and GU regions, respectively.

Therefore, the methodology of Silva et al. (2021) was adopted, in which for the parametric data sets ($p > 0.05$) the Pearson correlation coefficient (r) was calculated, and for the nonparametric data ($p < 0.05$), the correlation coefficient was calculated by Spearman (ρ).

In addition to validating the spatialized data, this procedure was carried out to identify the degree of correlation between precipitation (ANA) and GrW flow. Spearman's correlation (ρ) was used to investigate the relationship between climatic mechanisms and precipitation. Following the methodology of Caroletti et al. (2019), the correlation statistics between estimated and measured precipitation were analyzed with the corresponding pixel (CHIRPS) of the location of each rainfall station in GrW. The Nash-Sutcliffe coefficient (NS) described in Eq. 1 was used to analyze the efficiency of CHIRPS in representing observed precipitation (ANA) in GrW (KRAKAUER et al., 2013). NS statistic classifies the estimated data as optimal when the calculation result exceeds 0.90 (RATA et al., 2020).

$$NS = 1 - \frac{\sum_{i=1}^n (P_{Est} - P_{Obs})^2}{\sum_{i=1}^n (P_{Obs} - \bar{P}_{Obs})^2} \quad (\text{Eq. 1})$$

To detect whether the samples come from the same population, that is, whether the rainfall observation stations in GrW are under the influence of different rainfall regimes (BOUGARA et al., 2020), we first relied on the results of the Shapiro-Wilk test that indicated the series of precipitation data from some rainfall stations that did not show a normal distribution. Therefore, the recommendations of Ye and Ahammed (2020) were considered, which discouraged the use of ANOVA due to its requirement for data normalization. Instead, the Kruskal-Wallis (KW) test, a calculation (Eq. 2) better suited for nonparametric data, was employed. A significance level of 5% ($p < 0.05$) was considered for KW, in which the null hypothesis (H_0) indicates that there is no detection of different rainfall regimes acting on GrW, and the alternative hypothesis (H_a) means that there is the influence of different rainfall regimes (BOUGARA et al., 2020).

$$T = \frac{12}{N(N+1)} \sum_{j=1}^k \frac{R_j^2}{n_j} - 3(N+1) \quad (\text{Eq. 2})$$

R_j is all ratings for the sample, n_j is the sample size, k is the number of samples, and N is the total sample size.

The Mann-Kandall (MK) test was used to verify whether there are upward or downward trends in historical weather series (ALEMU; DIOHA, 2020) in GrW. Associated with MK, Kendall's Tau statistic (τ) was also calculated and taken into account to check for hydro climatological changes (ASFAW et al., 2018), in which, according to Ely and Dubreuil (2017) the range (-1 to +1) indicates whether the trend is increasing (+) or decreasing (-). For MK, a significance level of 5% was adopted ($p < 0.05$), and H_0 and H_a were tested.

To perform the MK statistics, it was necessary to calculate (Eq. 3 and Eq. 4) the Sign (S) of the hydro climatological series from the sum of the S of the difference of all the values of the data under analysis (x_i) about the data later (x_i). If $S > 0$ ($S < 0$), the following measurements of the hydro climatological time series tend to be greater (smaller) than the previous measurements, this means that there are trends of increase (decrease) of the analyzed series (ALEMU; DIOHA, 2020).

$$S = \sum_{i=1}^{n-1} \sum_{j=n+1}^n 1 S(x_j - x_i) \quad (\text{Eq. 3})$$

$$\text{Signal (S)} = \begin{cases} +1 & \text{if } (x_j - x_i) > 0 \\ 0 & \text{if } (x_j - x_i) = 0 \\ -1 & \text{if } (x_j - x_i) < 0 \end{cases} \quad (\text{Eq. 4})$$

When the number of observations exceeds 10, the S statistic is approximately distributed with the mean (KENDALL, 1975). Eq. 5 describes the variance (Var (S)).

$$\text{Var (S)} = \frac{n(n-1)(2n+5) - \sum t(t-1)(2t+5)}{18} \quad (\text{Eq. 5})$$

n is the number of terms, and t is the number of equal terms.

The calculation (Eq. 6) of the Z_{MK} statistic, where the result consists of positive (negative) values, means that there are increasing (decreasing) trends in the hydro climatological series (SALVIANO et al., 2016). For H_a to be accepted, it is necessary to obtain a Z_{MK} value > 1.96 for a 95% confidence level (SALVIANO et al., 2016).

$$Z_{MK} = \begin{cases} \frac{S-1}{\sqrt{\text{Var}(S)}}, & \text{if } S > 0 \\ 0, & \text{if } S = 0 \\ \frac{S+1}{\sqrt{\text{Var}(S)}}, & \text{if } S < 0 \end{cases} \quad (\text{Eq. 6})$$

For this GrW study, only the most intense episodes of weather phenomena in extreme years (surplus and water shortages) were analyzed. Concomitant to the period of climatic phenomena, the wettest and driest years were classified based on the results of the calculation of the Rainfall Anomaly Index (RAI) described in Eq. 7 (ROOY, 1965; JORGE; LUCENA, 2018) in the study period (1981-2020).

$$\text{RAI} = \pm \frac{p-p'}{e-p'} \quad (\text{Eq. 7})$$

p is the measured precipitation (mm/year); p' is the average of the measured precipitation; and e is the 10 highest measured rainfall.

The climatic phenomena associated with extreme rainfall events were studied in years of EN and LN comprised between 1982-2019 and 1984-2018, respectively.

AD⁺ (1981, 1983, 1992, 1997, 2010, 2012) and AD⁻ (1984, 1985, 1986, 1989, 1991, 1994, 2009, 2014 and 2019). The spatial rainfall variability of extreme years was mapped in a Geographic Information System (GIS) environment, based on CHIRPS (BELAY et al., 2019).

3. RESULTS

3.1 – Validation: statistical correlation

Validation of estimated data (NS = 0.97-0.99) showed satisfactory results. All stations (AB, FRZ, KZ, Gu, Pgm and Cz) have high correlations ($r > 0.90-0.96$). Such correlations indicate that the CHIRPS product represents excellent quality and proximity to the precipitation observed in GrW. Tab. 1 shows the correlation between the variables that make up the ocean-atmosphere interactions. Attention is drawn to the TP moderate positive correlation between ONI and AB precipitation ($\rho = 0.53$), as well as ONI and Cz precipitation ($\rho = 0.46$). This implies a significant influence of the TP on the rainfall patterns in these áreas.

The TA showed stronger correlations over the TP. A highly negative correlation was observed between TNaxAB ($\rho = -0.88$) and TNaxPgm ($\rho = -0.93$), indicating that higher SST in the northern sector of the TA corresponded to lower precipitation in AB and Pgm. TNA relation with the other locations was classified as negatively strong. In the Southern part of the TA, strong and positive correlations were obtained between TSaxAB ($\rho = 0.83$) and TSaxPgm ($\rho = 0.80$). The other locations are also strong and positive, however, with a lower coefficient.

Table 1 – Correlation statistics: Climate indices and Rainfall.

	AB	FRZ	KZ	Gu	Pgm	Cz
	<i>SST x Rainfall (ρ)</i>					
<i>ONIxRainfall</i>	0.53	0.21	0.13	0.11	0.31	0.46
<i>TNaxRainfall</i>	-0.88	-0.90	-0.83	-0.90	-0.93	-0.93
<i>TSaxRainfall</i>	0.83	0.74	0.68	0.74	0.80	0.75
	<i>GU</i>			<i>GL</i>		
	<i>Rainfall x Flow (ρ)</i>					
ρ	0.58			0.89		

Source: Authors (2022). *GU: AB_{lower} station. GL: FRZ_{upper} station.

In the GrW, there is a significant difference in the correlation between observed precipitation and flow. The GU region showed a moderately positive correlation ($\rho = 0.58$).



However, in the GL there was a strong positive correlation ($\rho = 0.89$), i.e., precipitation and flow are directly proportional - with a greater volume of rain, river discharge also tends to increase.

3.2 – Kruskal-Wallis test

The Kruskal-Wallis nonparametric test, as shown in Tab. 2, detected that certain samples do not belong to the same population. In this case, H_0 was rejected, and H_a was accepted, which means that different rainfall regimes influence some rainfall stations in GrW ($p < 0.05$) referring to five stations: AB-FRZ ($\Delta R = 80.0$; $z = 5.1$), AB-KZ ($\Delta R = 49.3$; $z = 3.4$), AB-Gu ($\Delta R = 82.7$; $z = 5.7$), FRZ-Cz ($\Delta R = 60.0$; $z = 3.7$) and Gu-Cz ($\Delta R = 62.8$; $z = 4.2$).

Table 2 – Detection of significant difference in GrW rainfall.

$H_{GL} = 47.6$	AB-FRZ	AB-KZ	AB-Gu	FRZ-Cz	Gu-Cz
	Rainfall				
ΔR	80.0	49.3	82.7	60.0	62.8
z	5.1	3.4	5.7	3.7	4.2

Source: Authors (2022). * $p < 0.05$.

3.3 – Mann-Kendall test

Tab. 3 describes the trend analysis results of changes in hydro climatological variables. Unlike the ONI, the climatic indices TNA ($S = 274$; $MKz = 3.18$) and TSA ($S = 235$; $MKz = 2.72$) showed increasing trends over the years. In the precipitation, the highlights are the trend of increasing precipitation in the FRZ pluviometric stations ($S = 108$; $MKz = 2.0$; Sen's slope = 20.0) and decreasing in the KZ pluviometric stations ($S = -171$; $MKz = -2.0$; Sen's slope = -20.0). The other locations and variables analyzed did not obtain the necessary combination of statistical parameters for a more decisive definition of their respective trends.

Table 3 – Detection of trends in hydroclimatic changes.

	<i>S</i>	<i>Var (S)</i>	τ	<i>Sen'slope</i>	<i>MK_z</i>	<i>p-value</i>
<i>Climate Indices</i>						
<i>ONI</i>	-38	7364.6	-0.05	-0.003	0.43	0.66
<i>TNA</i>	274	7366.6	0.35	0.010	3.18	0.001
<i>TSA</i>	235	7363.0	0.30	0.010	2.72	0.006
<i>Rainfall</i>						
<i>AB</i>	94	7366.6	0.12	1.1	12.7	0.281
<i>FRZ</i>	108	2842.0	0.26	2.0	20.0	0.044
<i>KZ</i>	-171	6833.6	-0.23	-2.0	-13.9	0.039
<i>Gu</i>	-44	7366.6	-0.05	-0.5	-4.1	0.619
<i>Pgm</i>	11	6833.6	0.01	0.1	1.6	0.904
<i>Cz</i>	-89	4958.3	-0.15	-1.2	-8.2	0.213
<i>Flow</i>						
<i>GU</i>	0	2842.0	0	0	0	0.985
<i>BL</i>	62	7366.6	0.079	0,7	0,7	0.480

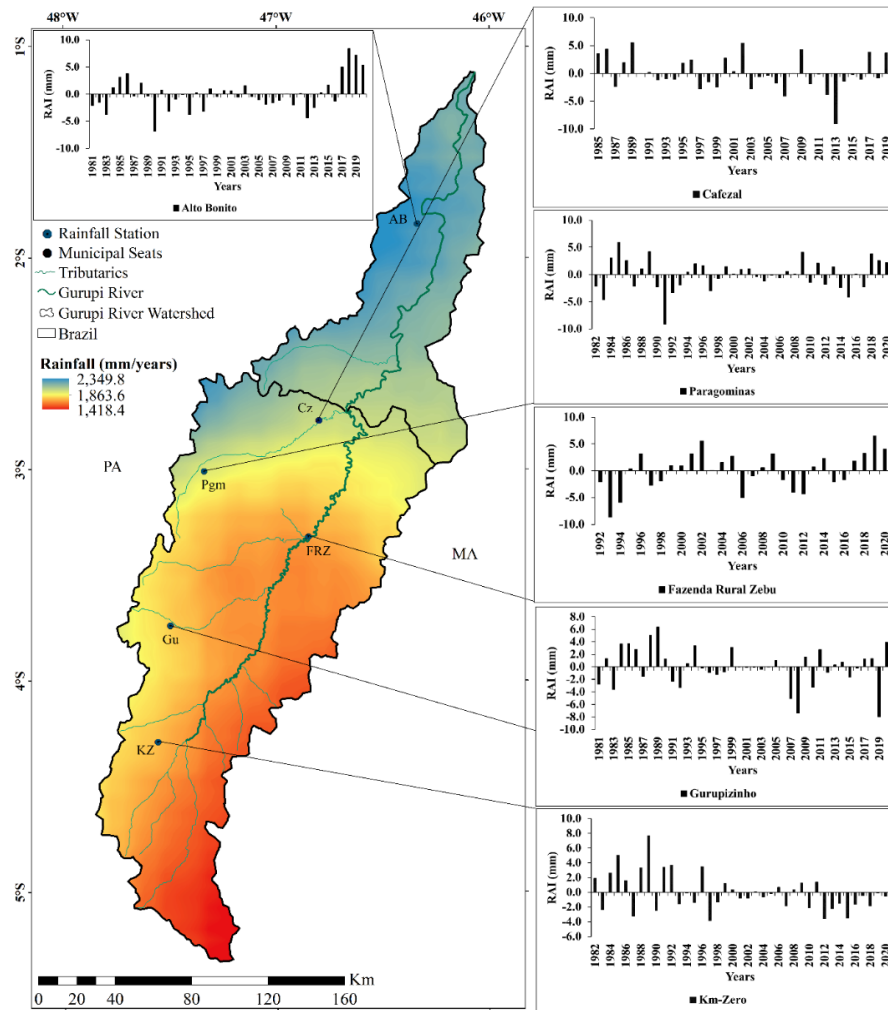
Source: Authors (2022). *GU: AB_{lower} station. GL: FRZ_{upper} station.

3.4 – Rainfall

Fig. 2 displays the spatial variability of precipitation (1981-2021) in the GrW region, represented by the annual RAI. The highest precipitation values (2,349.8 mm) are observed in the BG region, while the AG region exhibits a lower rainfall pattern (1,418.4 mm). Notably, observed precipitation at specific points, such as the BG region, demonstrates an increasing trend in rainfall volume, particularly in recent years (2017-2020). During this period, there are high anomalous values ranging from 5.0 mm to 8.4 mm, which classify these years as extremely rainy, influenced by the AD⁻ and LN phenomena.

However, it is important to emphasize that the GrW region presents significant spatiotemporal variability in rainfall, which directly influences water availability. Specifically, the GU region shows specific local indicators of declining precipitation trends, i.e., a reduction in rainfall recharge over the years. Notable years in this regard include 2010 (-3.2 mm), 2012 (-4.3 mm) and 2015 (-4.1 mm), which were characterized as very dry and extremely dry periods influenced by AD⁺ and EN events.

Figure 2 – Rainfall space-time variability: Gurupi river Watershed.

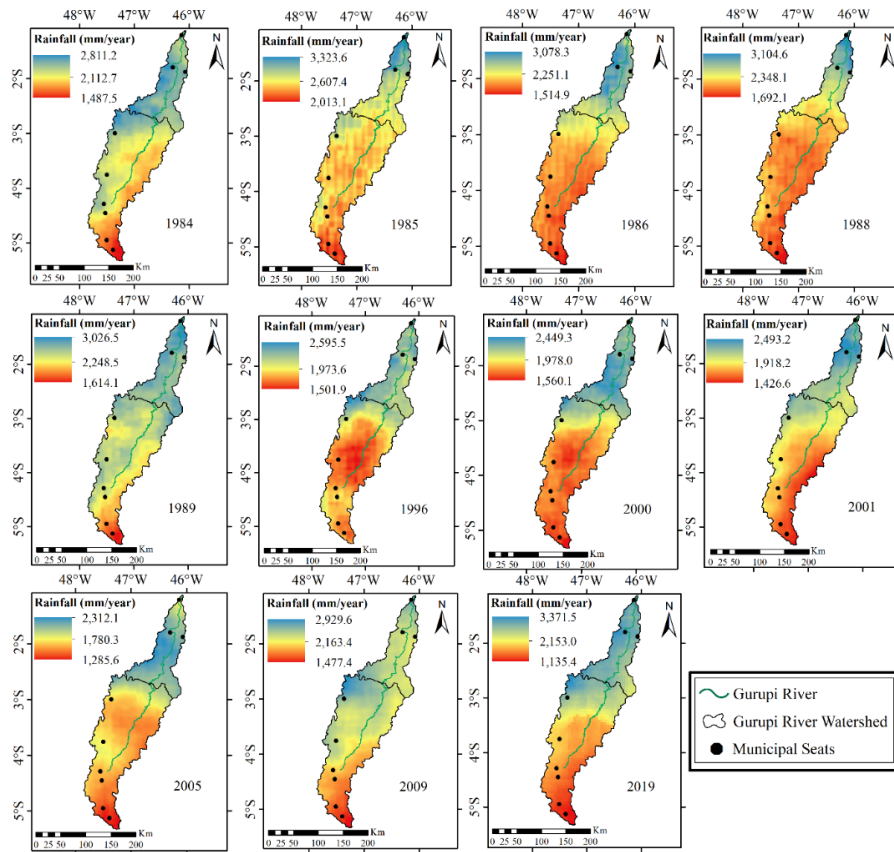


Source: Authors (2022). *MA-State of Maranhão; PA-State of Pará.

3.5 – Rainfall: rainy years (LN/AD⁻)

The spatiotemporal rainfall variability in rainy years (Fig. 3) is generally influenced by climatic mechanisms arising from the ocean-atmosphere interaction, in which some phases of these phenomena contribute to an increase in precipitation. In the extreme years in which the LN and AD⁻ phenomena occurred, the highest volumes of precipitation were concentrated in the GL region (North).

Figure 3 – Rainfall space-time variability in extreme years (LN|AD⁻): Gurupi River watershed.



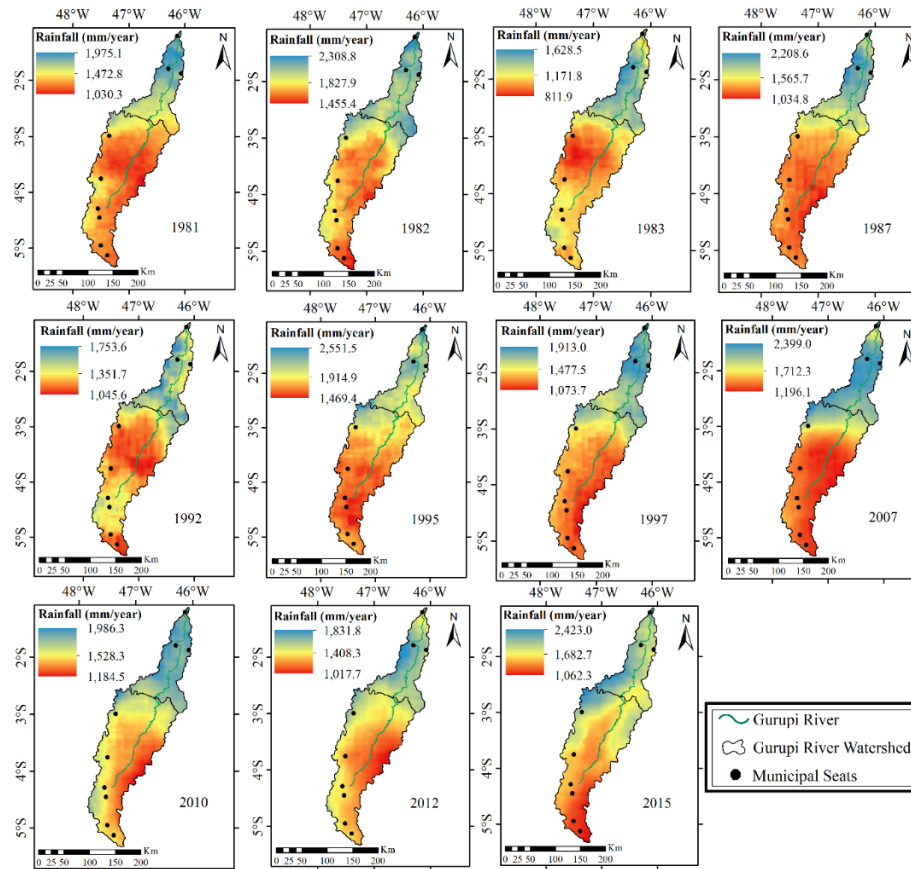
Source: Authors (2022).

In 1985 (3,323.6 mm) and 2019 (3,371.5 mm), the highest precipitation values were recorded. The extreme year 1985 was associated with the LN and AD⁻ events that occurred. In contrast, 2019 presented a different scenario, as it experienced the influence of EN, but with a likely greater impact from AD⁻ during that period.

3.6 – Rainfall: dry years (EN/AD⁺)

The spatiotemporal variability of precipitation in dry years (Fig. 4) is strongly related to the climate modes of the TA and TP oceans, where the phase of these events contributes to the inhibition of precipitating clouds formation. In dry years impacted by EN and AD⁺, precipitation along the GrW is spatially distributed, in general, with few differences in previous observations (Fig. 2 e Fig. 3). However, rainfall was greatly reduced in dry years, as in 1983 (811.9 mm) and 2012 (1,017.7 mm) which reached minimum values in other years. The atmospheric forcings that inhibit precipitation, such as EN and AD⁺, may have favored low rainfall in 1983. The AD⁺ in 2012 contributed to the decrease in rainfall this year.

Figure 4 – Rainfall space-time variability in extreme years (EN | AD⁺): Gurupi River watershed.

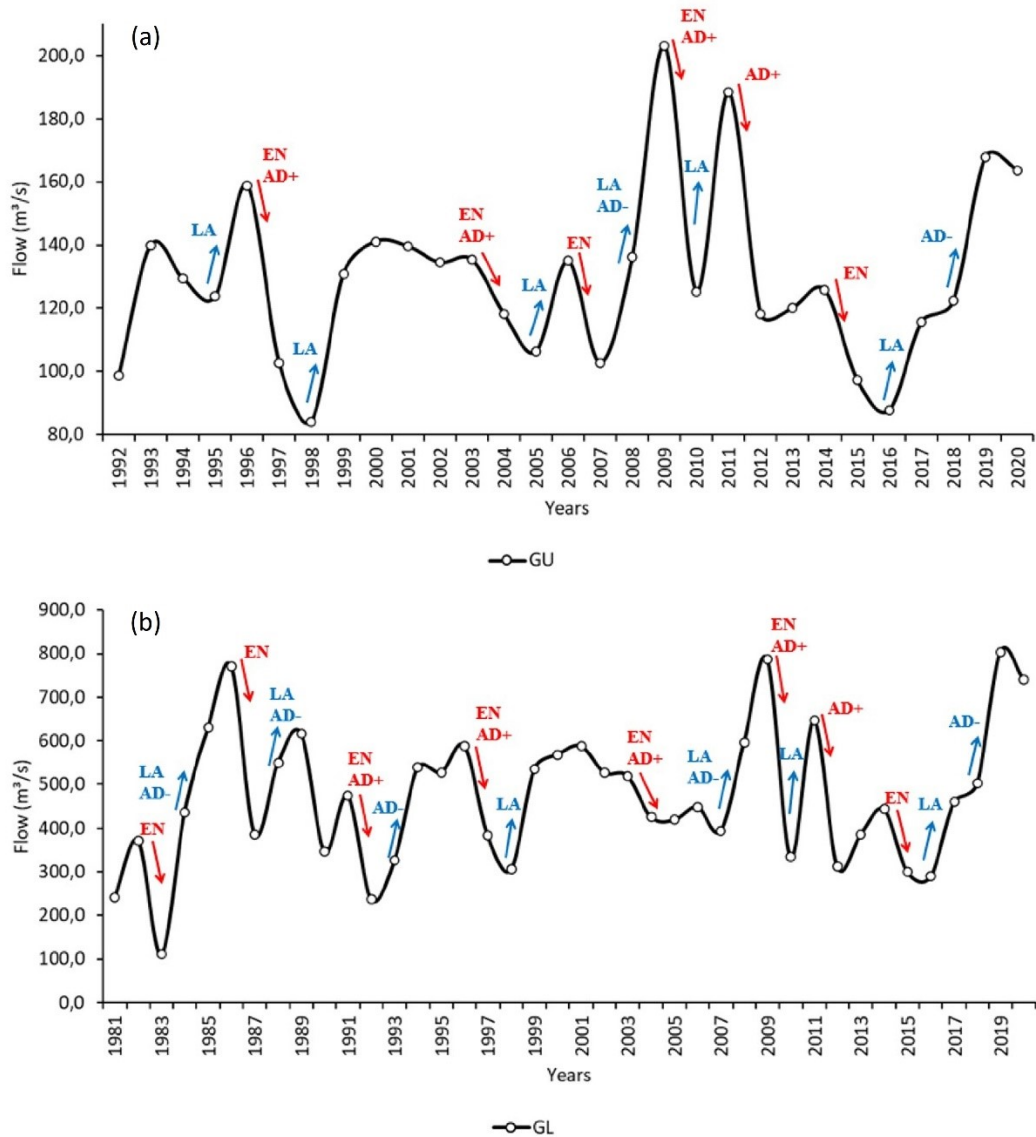


Source: Authors (2022).

3.7 – River regime

The fluviometric variability of the Gurupi River is characterized by an increasing trend over the years, mainly in the GL region. In Fig. 5a, a decline was identified from 1996 (158.8 m³/s) and reached a minimum value in 1998 (84.1 m³/s), the lowest flow rate observed in the historical series with a sharp reduction of 74.7 m³/s in 2 years. Another highlight was in 2016 (87.6 m³/s), where the GU region recorded one of the lowest minimum flow measurements. This drop in river flow was caused by the reduction in precipitation indicated by negative RAI in periods of the strongest EN events. The highest peaks in discharges in this stretch of the Gurupi River occurred in 2009 (203.2 m³/s) and 2011 (188.4 m³/s). Despite the climatic conditions (LN and AD⁻) influencing the rainfall in these years, only in 2009, a RAI favored an increase in the flow intensity. It is worth noting that in these years, the rapid growth in flow values from 2007 (102.7 m³/s) to the peak in 2011 was driven by phenomena (LN and AD⁻) and resulted in an increase of 100.5 m³/s.

Figure 5 – River temporal variability of the (a) GU e (b) GL: Gurupi River watershed.



Source: Authors (2022). *GU-Gurupi Upper; GL-Gurupi Lower; EN-El Niño; LN-La Niña; AD⁺ - Positive Atlantic Dipole; AD⁻ - Negative Dipole Atlantic.

Fig. 5b shows the GL as the sector of the GrW where the minimum flow occurred in 1983 ($110.9 m^3/s$) and 1992 ($237.6 m^3/s$). However, the most abrupt flow drops were 1986-87 ($384.3 m^3/s$) and 2009-10 ($452.1 m^3/s$). Such reductions in the river flow were caused by the EN and AD⁺ phenomena that possibly hampered the convective activity in the region, causing negative RAI in those years. However, maximum flow values are highlighted in the years 1986 ($770.2 m^3/s$), 2009 ($786.8 m^3/s$) and 2019 ($803.6 m^3/s$). However, river discharges in 1983-86 ($659.3 m^3/s$) and 2016-19 ($514.7 m^3/s$) were the highest observed increase. LN and AD⁻ events in these years are highly related to precipitation in this area, which generated an increase in water recharge according to the RAI of the years 1986, 2009, and 2019.



4. DISCUSSION

The greater rainfall in the Northern sector of GrW (as shown in Fig. 2, Fig. 3 and Fig. 4) is likely attributed to its proximity to the coast. This region receives the majority of moisture incursion from the AT due to the Northeast trade winds and is additionally influenced by sea breezes, which prepare the atmosphere for precipitation formation.

Significant correlations with the climatic mechanisms of both oceans (TP and TA) observed in this study corroborate the evidence about the great influence of the phenomena of the ocean-atmosphere interaction. Considering the correlations, a stronger impact of ENSO on the precipitation in the GL region is evident. However, the warming trend of the TA and the high correlation with precipitation suggest that the climatic mechanisms of this part of the ocean could impact and even change the annual rainfall distribution. Trends of changes in GrW precipitation are observed southwest of GrW, indicating the decline of this variable on an annual and monthly scale (December and January).

GrW is more sensitive to AD⁻ events, such as the rainy years reported by Integrated Natural Disaster Information System (S2iD, 2022). In addition, this TA phenomenon contributed to a greater frequency and intensity of rainfall observed in the years 1985 (KZ and Pg), 1989 (KZ, Gu, Pg and Cz), 2009 (Pg and Cz), 2019 (AB and FRZ). According to reports from S2iD (2022), in 2019, an emergency situation alert was caused by five episodes of heavy rain in the GrW region. Such information suggests that the 2019 AD⁻ had an impact on the precipitation of GrW, especially in the GL region. Other cases of natural disasters were reported by S2iD (2022), however, in years with lower anomalous precipitation values. It is necessary to report that in 1991 (Pg), 1994 (FRZ), 2013 (Cz), 2008 (Gu) and 2019 (Gu), the RAI values were not taken into account because they were the years with the greatest absence of observations in the respective rainfall stations.

The TP weather phenomena had different impacts on GrW precipitation. The LN presented higher frequency and intensity of signals in the years 1985 (KZ and Pg), 1988 (Gu), 1989 (KZ, Gu, Pg and Cz), 2009 (Pg and Cz), 2017 (AB) and 2018 (AB) categorized as extremely rainy. The S2iD (2022) declared an Emergency Situation in 2009 (LN) in some municipalities that are part of the GrW, due to the occurrence of floods and erosive processes, natural disasters that are associated with heavy rains (S2iD, 2022). According to the S2iD (2022), the

year 2011 was marked by the LN analyzed in this research, a period in which there were records of floods in the GrW.

Among the EN events, the strongest signals classified as extremely dry were only in the years 1983 (Pg), 2007 (Cz), 2015 (Pg). Therefore, the EN phenomenon, when classified as strong (JIMENÉZ-MUÑOZ et al., 2016) does not only contribute to the inhibition of rain during the period of action of the phenomenon (CAI et al., 2020). Indirectly, extreme droughts associated with EN decrease the rate of evapotranspiration into the atmosphere, leading to decreased precipitation (COSTA et al., 2018), as observed South of the GrW. Marengo et al. (2022) attributed this drought scenario in GrW to climatic pressure associated with the advance of the agricultural frontier. This factor results in delays at the onset of the rainy season and drier days due to the effect of air subsidence in the region, despite the presence of a greater number of rainy years, as indicated by observations in the GrW.

However, projections suggest that the anomalous heating of the TA will lead to increased moisture transport to the Amazon region, promoting higher rainfall with intensified convection (GOMES et al., 2022). This aligns with the statistical findings (MKz) of the current study. Precipitation in GrW showed a greater tendency to the effects of AD⁻ events, but it is worth mentioning that precipitation has a greater statistical correlation with TNA oscillations, the same observations made by Jimenez et al. (2019). Similar results were reported by Jimenez et al. (2018), however, the researchers reported that strong AD⁺ and EN events caused a reduction in cloud cover in the transition region from the Amazon to the Cerrado and may intensify their effects in extreme years where both occur simultaneously. The decrease in rainfall was identified at the KZ station. These interactions are ratified by Schumacher et al. (2022) when they suggest that even in years of strong EN, droughts in the Amazon are more associated with AD⁺ events, information that agrees with some results of this research since GrW has a greater correlation with the Northern part of the TA, which may favor the formation of AD⁺ with the anomalous heating trends of this sector of the TA ocean.

Therefore, Amazon rivers are impacted by the effects of ocean-atmosphere interactions (JAHFER et al., 2017). This teleconnection, which examines the impact of ocean-atmosphere coupling on the fluvial regime, was analyzed for the Amazon (BARICHIVICH et al., 2018). It takes into account the influence of ascending winds in increasing rainfall and, consequently, leading to extreme flood events.



These findings corroborate the results found in this study, especially in the GU region, where the hydrometeorological variables being analyzed exhibit significantly strong correlations with the climatic mechanisms of the TA. The influence of the climatic mechanisms of both oceans is observed in the fluvial regime of the GU and GL, marked by peaks and abrupt reductions in the extreme years.

5. FINAL CONSIDERATIONS

The proximity of the GrW from the coast is, likely, a determining factor for higher rainfall, which may promote greater susceptibility to events related to TA. In addition, KW indicated at least two rainfall regimes in GrW. Extremes events were well detected by RAI and CHIRPS. Some years of extreme rainfall did not occur during the periods of activity of the ENSO and AD phenomena, this raises the hypothesis that other climatic mechanisms may have contributed to greater convective activity in the GrW region. The years 1983, 1989, and 2019 were the most severe, with the highest frequency and intensity in the extreme values of the RAI. Unlike other years, 2019 only had one event, the AD⁻, which reflects how vulnerable GrW is to this phenomenon.

TNA had the greatest influence on GrW precipitation, followed by TSA, with high correlational values for most stations. The precipitation of the AB station has a greater relationship with the flow of the GL, in addition to capturing that the AB presents greater differences in the normal distribution of precipitation about the other stations and with trends of changes towards growth in the local rainfall regime.

These findings serve as a warning to the municipality of Viseu, as there is much evidence that it is vulnerable to hydro climatological extremes. Other trends in precipitation changes that stand out are in the FRZ and KZ stations. This highlights the considerable instability of precipitation in the transition region of the GrW biome, where two points in the GU sector exhibit contrasting variability trends.

Some years marked by climatic phenomena may be associated with a reduction in water supply and a lag in the Gurupi River. Greater hydroclimatic monitoring in GrW needs to be a priority since real data contribute to greater assertiveness and precision in making

decisions related to analyzing hydroclimatic forecast models, in addition to mitigating the impacts of human actions that enhance the effects of climate extremes.

ACKNOWLEDGEMENTS

Amazon Foundation for Studies and Research Support (FAPESPA). Center for Research Applied to Regional Development (NUPAD).

REFERENCES

ALEMU, Z. A.; DIOHA, M. Climate change and trend analysis of temperature: the case of Addis Ababa, Ethiopia, **Environmental Systems Research**, v. 9, n. 27, p. 1-15, 2020.

ANA .Agência Nacional de Águas e Sanemanto Básico. (2021, 4 de Dezembro). Retrieved in <https://www.snirh.gov.br/portal/centrais-de-conteudos/conjuntura-dos-recursos-hidricos/conjuntura-dos-recursos-hidricos>.

Agência Nacional de Águas e Sanemanto Básico - ANA. Sistema Nacional de Informações sobre Recursos Hídricos. (2021, 4 de Dezembro). Retrieved in <http://www.snirh.gov.br/hidroweb/>.

ARAÚJO, R. G.; ANDREOLI, R. V.; CANDIDO, L. A.; KAYANO, M. T.; SOUZA, R. A. F. A influência do evento El Niño – Oscilação Sul e Atlântico Equatorial na precipitação sobre as regiões norte e nordeste da América do Sul. **Acta Amazônica**, v. 43 n. 4, p. 469-480, 2013.

ASFAW, A.; SIMANE, B.; HASSEN, A.; BANTIDER, A. Variability and time series trend analysis of rainfall and temperature in northcentral Ethiopia: a case study in Woleka sub-basin. **Weather and Climate Extremes**, v. 19, p. 29-41, 2018.

BAHAGA, T. K.; FINK, A. H.; KNIPPERTZ, P. Revisiting interannual to decadal teleconnections influencing seasonal rainfall in the Greater Horn of Africa during the 20th century. **International Journal of Climatology**, v. 39, n. 5, p. 2765-2785, 2019.

BARICHIVICH, J.; GLOOR, E.; PEYLIN, P.; BRIENEN, R. J. W.; Schongart, J.; Espinoza, J. C.; Pattnayak, K. C. Recent intensification of Amazon flooding extremes driven by strengthened Walker circulation. **Science Advances**, v. 4, n. 9, p. 1-7, 2018.

BELAY, A. S.; FENTA, A. A.; YENEHUN, A.; NIGATE, F.; TILAHUN, S. A.; MOGES, M. M.; DESSIE, M.; ADGO, E.; NYSSSEN, J.; CHEN, M.; VAN GRIENSVEN, A.; WALRAEVENS, K. Evaluation and application of multi-source satellite rainfall product CHIRPS to assess spatio-temporal rainfall variability on data-sparse western margins of Ethiopian highlands. **Remote Sensing**, v. 11 n. 22, p. 1-22, 2019. <https://doi.org/10.3390/rs11222688>.

BOUGARA, H.; HAMED, K. B.; BORGEMEISTER, C.; TISCHBEIN, B.; KUMAR, N. (2020). Analyzing trend and variability of rainfall in the Tafna basin (Northwestern Algeria). **Atmosphere**, v. 11, n. 4, p. 1-24, 2020. <https://doi.org/10.3390/atmos11040347>.

BRITO, A. P.; SILVA, N. C.; TOMASELLA, J.; FERREIRA, S. J. F.; MONTEIRO, M. T. F. Análise do Índice de Anomalia de Chuva e tendência de precipitação para estações pluviométrica na Amazônia central. **Revista Brasileira de Meteorologia**, v. 37, n. 1, p. 19-30, 2022.

CAI, W.; MCPHADEN, M. J.; GRIMM, A. M.; RODRIGUES, R. R.; TASCHETTO, A. S.; GARREAU, R. D.; DEWITTE, B.; POVEDA, G.; HAM, Y.; SANTOSO, A.; NG, B.; ANDERSON, W.; WANG, G.; GENG, T.; JO, H.; MARENGO, J. A.; ALVES, L. M.; OSMAN, M.; LI, S.; WU, L.; KARAMPERIDOU, C.; TAKAHASHI, K.; VERA, C. Climate impacts of the El Niño-Southern Oscillation on South America. **Nature Reviews Earth & Environment**, v. 1, p. 215-231, 2020.

CAPOZZOLI, C. R.; CARDOSO, A. O.; FERRAZ, S. E. T. Padrões de variabilidade de vazão de rios nas principais bacias brasileiras e associações com índices climáticos. **Revista Brasileira de Meteorologia**, v. 32, n. 2, p. 243-254, 2017. <https://doi.org/10.1590/0102-77863220006>.

CAROLETTI, G. N.; COSCARELLI, R.; CALOIERO, T. Validation of satellite, reanalysis and RCM data of Monthly rainfall in Calabria (Southern Italy). **Remote Sensing**, v. 11, n. 13, p. 1-20, 2019.

CAROLETTI, G. N.; COSCARELLI, R.; CALOIERO, T. A sub-regional approach to the influence analysis of teleconnection patterns on precipitation in Calabria (Southern Italy). **International Journal of Climatology**, v. 41, n. 9, p. 4574-4586, 2021. <https://doi.org/10.1002/joc.7087>.

Climate Hazards Group InfraRed Precipitation with Stations - CHIRPS. Climate Hazard Center – UC Santa Bárbara. (2021, 11 de Dezembro). Retrieved in https://data.chc.ucsb.edu/products/CHIRPS-2.0/global_annual/tifs/.

COSTA, A. C. L.; ROWLAND, L.; OLIVEIRA, R. S.; OLIVEIRA, A. A. R.; BINKS, O. J.; SALMON, Y.; VASCONCELOS, S. S.; SILVA JUNIOR, J. A.; FERREIRA, L. V.; POYATOS, R.; MENCUCCINI, M.; MEIR, P. Stand dynamics modulate water cycling and mortality risk in droughted tropical forest. **Global Change Biology**, v. 24, n. 1, p. 249-258, 2018.

COSTA, J.; PEREIRA, G.; SIQUEIRA, M. E.; CARDOZO, F. Validação dos dados de precipitação estimados pelo CHIRPS para o Brasil. **Revista Brasileira de Climatologia**, v. 24, p. 228-243, 2019.

ELY, D. F.; DUBREUIL, V. Análise das tendências espaço-temporais das precipitações anuais para o estado do Paraná – Brasil. **Revista Brasileira de Climatologia**, v. 21, p. 553-569, 2017.

FUNK, C.; PETERSON, P.; LANDSFELD, M.; PEDREROS, D.; VERDIN, J.; SHUKLA, S.; HUSAK, G.; ROWLAND, J.; HARRISON, L.; HOELL, A.; MICHAELSEN, J. The climate hazards infrared precipitation with stations – a new environmental record for monitoring extremes. **Scientific Data**, v. 2, n. 150066, 2015. <https://doi.org/10.1038/sdata.2015.66>.

Golden Gate Weather Services. (2021, July 12). Retrieved in <https://ggweather.com/enso/oni.htm>.

GOMES, G. D.; NUNES, A. M. B.; LIBONATI, R.; AMBRIZZI, T. Projections of subcontinental changes in seasonal precipitation over the two major river basins in South America under an extreme climate scenario. **Climate Dynamics**, v. 58, p. 1147-1169, 2022.

GONZALES, E.; INGOL, E. Determination of a new coastal ENSO oceanic index for Northern Peru. **Climate**, v. 9, n. 5, p. 1-23, 2021. <https://doi.org/10.3390/cli9050071>.

HAYASHI, M.; JIN, F.; STUECKER, M. F. Dynamics for El Niño-La Niña asymmetry constrain equatorial-Pacific warming pattern. **Nature Communications**, v. 11, n. 4230, p. 1-10, 2020.

Instituto Nacional de Meteorologia – INMET. **Normais Climatológicas**. (2022, August 19). Retrieved in https://clima.inmet.gov.br/NormaisClimatologicas/1961-1990/precipitacao_acumulada_mensal_anual.

JIMENÉZ, J. C.; LIBONATI, R.; PERES, L. Droughts over Amazonia in 2005, 2010, and 2015: a cloud cover perspective. **Frontiers in Earth Science**, v. 6, n. 227, p. 1-7, 2018.

JIMENÉZ, J. C.; MARENGO, J. A.; ALVES, L. M.; SULCA, J. C.; TAKAHASHI, K.; FERRETT, S.; COLLINS, M. The role of ENOS flavours and TNA on recent droughts over Amazon forests and the Northeast Brazil region. **International Journal of Climatology**, v. 41, n. 7, p. 3761-3780, 2019. <https://doi.org/10.3389/feart.2018.00227>.

JIMNÉZ-MUÑOZ, J. C.; MATTAR, C.; BARICHIVICH, J.; SANTAMARÍA-ARTIGAS, A.; TAKAHASHI, K.; MALHI, Y.; SOBRINO, J. A.; SCHRIER, G. Record-breaking warming and extreme drought in the Amazon rainforest during the course of El Niño 2015-2016. **Scientific Report**, v. 6, n. 33130, p. 1-6, 2016. <https://doi.org/10.1038/srep33130>.

JAHFER, S.; VINAYACHANDRAN, P. N.; NANJUNDIAH, R. S. Long-term impact of Amazon river runoff on northern hemispheric climate. **Scientific Reports**, v. 7, n. 10989, p. 1-9, 2017.

JORGE, R. L. O.; LUCENA, D. B. Eventos extremos anuais de precipitação em Mauriti-CE. **Ciência & Natura**, v. 40, n. 65, p. 1-10, 2018. <https://doi.org/10.5902/2179460X34045>.

KENDALL, M. G. Rank correlation methods. **Oxford University Press**, Ed., 272, 1975.

KRAKAUER, N. Y.; PRADHANANG, S. M.; LAKHANKAR, T.; JHA, A. K. Evaluating satellite products for precipitation estimation in mountain regions: a case study for Nepal. **Remote Sensing**, v. 5, p. 4107-4123, 2013. <https://doi.org/10.3390/rs5084107>.

MARENGO, J. A.; JIMENEZ, J. C.; ESPINOZA, J.; CUNHA, A. P.; ARAGÃO, L. E. O. Increased climate pressure on the agricultural frontier in the Eastern Amazonia-Cerrado transition zone. **Scientific Reports**, v. 12, n. 457, p. 1-10, 2022.



MENDES, A. T.; ZUCOWSKI JUNIOR, J. C. Caracterização do regime pluviométrico do município de Araguaína-TO. **Revista Brasileira de Meteorologia**, v. 34, n. 4, p. 449-458, 2019.

MELLO, Y. R.; KOHLS, W.; OLIVEIRA, T. M. N. Uso de diferentes métodos para preenchimento de falhas em estações pluviométricas. **Boletim Geográfico**, v. 35, n. 1, p. 112-121, 2017.

MMA. Ministério do Meio Ambiente. **Caderno da Região Hidrográfica Atlântico Nordeste Ocidental** (2022, January 13). Retrieved in http://www.bibliotecaflorestal.ufv.br/bitstream/handle/123456789/3483/Parte-1-Caderno-da-Regi%C3%A3o-Hidrogr%C3%A1fica-Atl%C3%A2ntico-Nordeste-Ocidental_MMA.pdf?sequence=1.

NASCIMENTO, M. B.; ALMEIDA, N. V.; ARAÚJO, L. E. Análise da variabilidade da precipitação pluviométrica na microrregião de Umbuzeiro, Paraíba. **Revista Brasileira de Climatologia**, v. 26, n. 16, p. 233-248, 2020. <https://doi.org/10.5380/abclima.v26i0.65498>.

NIAZ, R.; ALMAZAH, M. M. A.; AL-DUAIS, F. S.; IQBAL, N.; KHAN, D. M.; HUSSAIN, I. Spatiotemporal analysis of meteorological drought variability in a homogeneous region using standardized drought indices. **Geomatics, Natural Hazards and Risk**, v. 13, n. 1, p. 1457-1481, 2022. <https://doi.org/10.1080/19475705.2022.2079429>.

NOAA. National Oceanic Atmospheric and Administration. **Climate Indices List**. (2021, Dezember 2). Retrieved in <https://psl.noaa.gov/data/climateindices/list/>.

NOBRE, G. G.; MUIS, S.; VELDKAMP, T. I. E.; WARD, P. J. Achieving the reduction of disaster risk by better predicting impacts of El Niño and La Niña. **Progress in Disaster Science**, v. 2, p. 1-6, 2019. <https://doi.org/10.1016/j.pdisas.2019.100022>.

OLAFSDOTTIR, H. K.; ROOTZÉN, H.; BOLIN, D. Extreme rainfall events in the Northeastern United States become more frequent with rising temperatures, but their intensity distribution remains stable. **Journal of Climate**, v. 34, n. 22, p. 8863-8877, 2021.

PEDREIRA JUNIOR, A. L.; QUERINO, C. A. S.; BIUDES, M. S.; MACHADO, N. G.; SANTOS, L. O. F.; IVO, I. O. Influence of El Niño and La Niña phenomena on seasonality of the relative frequency of rainfall in southern Amazonas mesoregion. **Revista Brasileira de Recursos Hídricos**, v. 25, p. 1-8, 2020. <https://doi.org/10.1590/2318-0331.252020190152>.

RATA, M.; DOUAOUI, A.; LARID, M.; DOUAIK, A. Comparison of geostatistical interpolation methods to map annual rainfall in the chéiff watershed, Algeria. **Theoretical and Applied Climatology**, v. 141, p. 1009-1024, 2020. <https://doi.org/10.1007/s00704-020-03218-z>.

REBOITA, M. S.; SANTOS, I. A. Influência de alguns padrões de teleconexão na precipitação no Norte e Nordeste do Brasil. **Revista Brasileira de Climatologia**, v. 15, p. 28-48, 2014.

REN, G.; CHAN, J. C. L.; KUBOTA, H.; ZHANG, Z.; LI, J.; ZHANG, Y.; ZHANG, Y.; YANG, Y.; REN, Y.; SUN., X.; SU, Y.; LIU, Y.; HAO, Z.; XUE, X.; QIN, Y. Historical and recent change in extreme climate over East Asia. **Climate Change**, v. 168, n. 22, p. 1-19, 2019.

RODRIGUES, B. D.; COUTINHO, M. D. L.; SAKAMOTO, M. S.; JACINTO, L. V. Uma análise sobre as chuvas no Ceará baseada nos eventos de El Niño, La Niña e no Dipolo do Servain durante a estação chuvosa. **Revista Brasileira de Climatologia**, v. 28, p. 507-519, 2019.

ROOY, M. P. V. A. rainfall anomaly index independent of time and space. Notes. **Weather Bureau of South Africa**, v. 14, p. 43-48, 1965.

RUEZZENE, C. B.; MIRANDA, R. B.; TECH, A. R. B.; MAUAD, F. F. Preenchimento de falhas em dados de precipitação através de métodos tradicionais e por inteligência artificial. **Revista Brasileira de Climatologia**, v. 29, p. 177-204, 2021.

SALES, D. P.; OLIVEIRA NETO, F. M. O. Análise da distribuição das queimadas no cerrado maranhense, Brasil (2014-2018). **Revista Meio Ambiente e Sustentabilidade**, v. 9, n. 18, p. 17-31, 2020. <https://doi.org/10.22292/mas.v9i18.880>.

SALVIANO, M. F.; GROppo, J. D.; PELLEGRINO, G. Q. Análise de tendências em dados de precipitação e temperatura no Brasil. **Revista Brasileira de Meteorologia**, v. 31, n. 1, p. 64-73, 2016. <https://doi.org/10.1590/0102-778620150003>.

SANTOS, F. A.; MENDES, L. M. S.; CRUZ, M. L. B. Avaliação de ocorrências de eventos climáticos extremos na sub-bacia hidrográfica do rio Piracuruca. **Revista GEOgrafias**, v. 28, n. 1, p. 43-61, 2020.

SANTOS, J. S.; ROCHA, E. J. P.; SOUZA JUNIOR, J. A.; SANTOS, J. S.; SANTOS, F. A. A. Climatologia da Amazônia Oriental: uso de prognósticos climáticos como ferramenta de prevenção de ameaças naturais. **Revista Brasileira de Geografia Física**, v. 12, n. 5, p. 1853-1871, 2019.

SCHUMACHER, V.; JUSTINO, F.; LEONARDO, N. F.; PEREIRA, M. P. Disentangling the role of the Pacific and Atlantic oceans during the Amazonian droughts in 2015. **Theoretical and Applied Climatology**, v. 148, p. 1057-1067, 2022. <https://doi.org/10.1007/s00704-022-03998-6>.

SILVA, G. M. F.; ZANCHI, F. B.; SILVA, J. B. L.; BERNARDES, M. E. C. Disponibilidade hídrica de uma bacia hidrográfica no sul da Bahia. **Revista Brasileira de Geografia Física**, v. 14, n. 3, p. 1597-1611, 2021. <https://doi.org/10.26848/rbgf.v14.3.p1597-1611>.

SIQUEIRA, A. H. B.; MOLION, L. C. B. Análises climáticas: o filtro Hodrick-Prescott aplicado aos índices atmosféricos da oscilação Sul e da oscilação do Atlântico Norte. **Revista Brasileira de Meteorologia**, v. 30, n. 3, p. 307-318, 2015. <https://doi.org/10.1590/0102-778620130579>.

Sistema Integrado de Informações sobre Desastres Naturais - S2iD. **Secretaria Nacional de Proteção e Defesa Civil**. (2022, July 07). Retrieved in <https://s2id.mi.gov.br/>.



SOUZA, E. B.; KAYANO, M. T.; AMBRIZZI, T. Intraseasonal and submonthly variability over the eastern Amazon and northeast Brazil during the autumn rainy season. **Theoretical and Applied Climatology**, v. 81, n. 3/4, p. 177-191, 2005.

TOWNER, J.; CLOKE, H. L.; LAVADO, W.; SANTINI, W.; BAZO, J.; PEREZ, E. C.; STEPHENS, E. M. Attribution of Amazon floods to modes of climate variability: a review. **Meteorological Applications**, v. 27, n. 5, p. 1-36, 2020. <https://doi.org/10.1002/met.1949>.

TOWNER, J.; FICCHI, A.; CLOKE, H. L.; BAZO, J.; PEREZ, E. C.; STEPHENS, E. M. Influence of ENSO and tropical Atlantic climate variability on flood characteristics in the Amazon basin. **Hydrology and Earth System Sciences**, v. 25, p. 3875-3895, 2021.

UVO, C. B.; REPELLI, C. A.; ZEBIAK, S. E.; KUSHNIR, Y. The Relationship between Tropical Pacific and Atlantic SST and Northeast Brazil Monthly Precipitation. **Journal of Climate**, v. 11, p. 551-562, 1998.

ZHANG, C.; HUANG, G.; YAN, D.; WANG, H.; ZENG, G.; WANG, S.; LI, Y. Analysis of South American climate and teleconnection indices. **Journal of Contaminant Hydrology**, v. 244, p. 1-15, 2022. <https://doi.org/10.1016/j.iconhyd.2021.103915>.

YE, Q.; AHAMMED, F. Quantification of relationship between annual daily maximum temperature and annual daily maximum rainfall in South Australia. **Atmospheric and Oceanic Science Letters**, v. 13, n. 4, p. 286-293, 2020.

YUN, K.; TIMMERMANN, A.; STUECKER, M. F. Synchronized spatial shifts of Hadley and Walker circulations. **Earth System Dynamics**, v. 12, p. 121-132, 2021.